2010 IEEE International Conference on Robotics and Automation
Anchorage Convention District
May 3-8, 2010, Anchorage, Alaska, USA

Control Design and Allocation of an Over-Actuated Triangular Floating Platform

Kostas Vlachos, and Evangelos Papadopoulos, *Senior Member, IEEE*

***Abstract*— This paper presents the design and practical implementation of an autonomous dynamic positioning scheme, i.e., the stabilization of linear and angular velocities as well as the position and orientation, of a novel triangular floating sea platform. The required closed-loop forces and moments must be provided by three rotating pump jets, located at the bottom of three partly submerged cylinders located at the three corners of the platform. With this control configuration the platform is over-actuated, i.e., it has more control inputs than degrees of freedom (DOF). Design rules that maximize the manipulability of the platform, and a control allocation scheme that allows goal realization without violating thruster capabilities are developed. Simulations results, including environmental disturbances, are presented that demonstrate the performance of the controller, and the allocation scheme employed.**

I. Introduction

FLOATING platforms are widely used in the offshore petroleum industry, as portable pipeline systems, as research, in-the-field laboratories, etc, [1]. To accomplish their task these platforms must be kept stationary at a desired position and orientation. Therefore, they are equipped with appropriate actuation systems that provide the necessary dynamic positioning to counterbalance the sea wave, wind and current induced forces and moments, and the uncertainties in modeling the dynamics of the platform. Floating platform dynamics are inherently nonlinear due to the rigid body dynamics and, more importantly, due to the strong hydrodynamic interactions, [2]. Hence, in order to design efficient closed-loop controllers, nonlinear techniques must be adopted. Control allocation schemes must also be designed; usually, such vessels have redundant actuators, i.e., they have more control inputs than DOF yielding an over-actuated control system. Thus, the closed-loop control forces and moments need to be efficiently distributed to the actuators in such a way that the control objective is realized without violating operational constraints (e.g. thrusters' capability). The above problem leads, in general, to a constrained optimization problem that is hard to solve using even state-of-the-art iterative numerical optimization software in a safety-critical real-time system with limiting processing capacity, [3]. Nevertheless, real-time iterative optimization solutions have been proposed [4], [5], and [6]. Optimal thrust allocation has been addressed in [7]. Thrusters that can be rotated, and thus produce two force components in the horizontal plane, are usually mounted under the hull of the vessel. Optimization schemes for such actuation configurations have been proposed for example in [8]. In [9], controllability problems regarding the plane motion were studied. The authors presented preliminary results on the subject in [10].

The aim of this work is the dynamic modeling and the stabilization of linear and angular velocities as well as of position and orientation, of a novel triangular floating platform, see Fig. 1. Our main goal is the practical implementation of such an autonomous dynamic positioning scheme, with real time capabilities.

Fig. 1. The triangular floating platform (under construction).

The required, closed-loop force and moment is provided by three rotating pump jets. The system is over-actuated, i.e., it has more control inputs than DOF. Hence, we design a properly control allocation scheme in order for the control objective to be realized without violating the thrusters capability. This scheme is based on the pseudo-inversion of the transformation matrix relating the control forces and the jets thrust. Furthermore, we formulate design rules that maximize the manipulability of the platform, based on the condition number of the normalized transformation matrix relating the control forces and the jets thrust.

This methodology provides a fast, reliable, and computationally inexpensive algorithm related to the complex, on-line, iterative ones. Simulation results, including sea current and wind forces, are presented to demonstrate the performance of the controller, and allocation scheme.

II. Platform System Description

A. General Description

The platform, which is under construction, is called "DELTA VERENIKI", and will be used during the assembly

Manuscript received February 08, 2010. This work was supported by the VERENIKI program with funding from the Hellenic Ministry of Education and Religion and the European Union.

K. Vlachos, and E. Papadopoulos are with the Department of Mechanical Engineering, National Technical University of Athens, 15780 Athens, Greece, (e-mail: {kostaswl; egpapado}@central.ntua.gr).

of the deep-sea high-energy neutrino telescope "NESTOR", [11], see Fig. 1. It consists of a triangular structure mounted on three double-cylinders, one at each corner of the structure. The plane of the triangle is parallel to the sea surface. These cylinders provide the necessary buoyancy since part of their body is immersed. The actuation of the platform is realized utilizing pump jets at the bottom of the three cylinders, fully submerged. A diesel engine drives each pump, while an electro-hydraulic motor can rotate the jet providing vectored thrust.

B. Geometry and Kinematics

The main body of the structure has the shape of an isosceles triangle with $L_{AB} = L_{AC}$, and L_{BC} the length of the base, see Fig. 2. The structure has its center of mass (CM) coinciding with point G, along the symmetry axis at a distance d_{AG} from the vertex A.

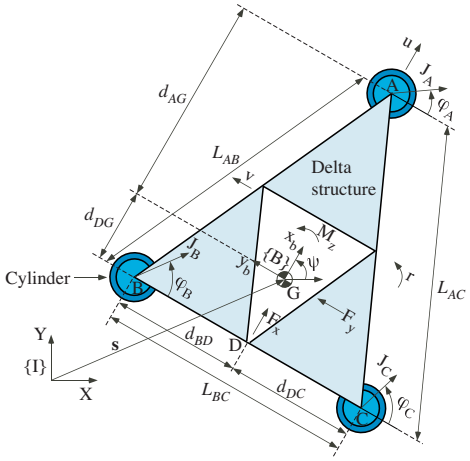

Fig. 2. A 2D representation of the platform.

To describe the kinematics of plane motion, two reference frames are employed, the inertial reference frame {I} and the body-fixed frame {B}, see Fig. 2. As shown, the origin of {B} frame coincides with the platform CM. The x_b body axis is aligned with the symmetry axis of the platform, the y_b points left, and z_b points upwards. Hence, the kinematics equations of the plane motion are:

$$\dot{\mathbf{x}} = \mathbf{R}\mathbf{v} \tag{1a}$$

where

$$\dot{\mathbf{x}} = [\dot{x}, \dot{y}, \dot{\psi}]^T \tag{1b}$$

$$\mathbf{v} = [u, v, r]^T \tag{1c}$$

$$\mathbf{R} = \begin{bmatrix} c\psi & -s\psi & 0 \\ s\psi & c\psi & 0 \\ 0 & 0 & 1 \end{bmatrix} \tag{1d}$$

with $s\cdot = sin(\cdot)$, $c\cdot = cos(\cdot)$. In (1), x and y represent the inertial coordinates of the CM and ψ the orientation of {B} with respect to the {I} frame; u and v are the surge and sway velocities respectively, defined in the body-fixed frame, and r is the yaw (angular) velocity of the platform, see Fig. 2.

Due to the fact that the hydrodynamics interactions are between the water and the submerged part of the cylinders, we also need the kinematics relations between the cylinders and the CM in order to derive equations for the hydrodynamic forces and moments. First, we introduce some necessary notations: ${}^B\mathbf{s}_{A/G}$ is the position of point A with respect to G expressed in frame {B}, and ${}^B\mathbf{s}_{B/G}$, and ${}^B\mathbf{s}_{C/G}$ have similar meaning; ${}^B\mathbf{v}_G = [u,v]^T$ is the linear velocity vector of the CM, ${}^B\mathbf{a}_G = {}^B(d\mathbf{v}/dt)_G$ is the linear acceleration vector, and $\alpha = dr/dt$ is the angular acceleration, all expressed in frame {B}. Then, the following geometric relations hold:

$${}^B\mathbf{s}_{A/G} = [d_{AG}, 0]^T \tag{2a}$$

$${}^B\mathbf{s}_{B/G} = [-d_{DG}, d_{BD}]^T \tag{2b}$$

$${}^B\mathbf{s}_{C/G} = [-d_{DG}, -d_{DC}]^T \tag{2c}$$

Velocities and accelerations are given by:

$${}^B\mathbf{v}_A = [u, \upsilon + rd_{AG}]^T \tag{3a}$$

$${}^B\mathbf{a}_A = [\dot{u} - r^2 d_{AG}, \dot{\upsilon} + \alpha d_{AG}]^T \tag{3b}$$

$${}^B\mathbf{v}_B = [u - rd_{BD}, \upsilon - rd_{DG}]^T \tag{3c}$$

$${}^B\mathbf{a}_B = [\dot{u} - \alpha d_{BD} + r^2 d_{DG}, \dot{\upsilon} - \alpha d_{DG} - r^2 d_{BD}]^T \tag{3d}$$

$${}^B\mathbf{v}_C = [u + rd_{DC}, \upsilon - rd_{DG}]^T \tag{3e}$$

$${}^B\mathbf{a}_C = [\dot{u} + \alpha d_{DC} + r^2 d_{DG}, \dot{\upsilon} - \alpha d_{DG} + r^2 d_{DC}]^T \tag{3f}$$

C. Dynamics

The structure oscillates in the vertical direction because of the weight and buoyancy equilibrium: specifically, when the weight of the structure increases –within certain bounds– the cylinders are submerged further, yielding increased buoyancy and vice-versa, see Fig. 3. The height of the cylinders above the surface is computed as:

$$h = H_{uc} - (1/R_{uc}^2)(m/(3\pi\rho) - R_{lc}^2 H_{lc}) \tag{4}$$

where ρ is the water density and m is the mass of the structure. Actuation and control in this direction is outside the scope of this work.

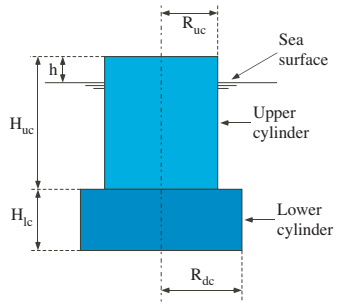

Fig. 3. A side view of the double-cylinder structure.

The hydrodynamic forces are due to the motion of the cylinders into the water: the added mass force is a linear function of the acceleration of the cylinder, while the drag force is a quadratic function of the cylinder velocity. These forces are modeled according to Morison's Equation [12]. As an example, we derive here the force on a cylinder at point A, expressed in body-fixed frame {B}:

$$\begin{aligned} \mathbf{f}_A = &-C_A\pi\rho[R_{uc}^2(H_{uc} - h) + R_{lc}^2 H_{lc}]\,{}^B\mathbf{a}_A \\ &- C_D\rho[R_{uc}(H_{uc} - h) + R_{lc}H_{lc}]\left\|{}^B\mathbf{v}_A\right\|{}^B\mathbf{v}_A \end{aligned} \tag{5}$$

where C_A is the added mass coefficient and C_D the drag coefficient. The forces on the cylinder are equivalent with an equal force and a moment acting on the CM. For example, the force in (5) gives

$$\boldsymbol{\tau}_G = {}^B\mathbf{s}_{A/G} \times \mathbf{f}_A \tag{6}$$

It is already mentioned that the jets can provide vectored thrust and thus more flexibility in control design, Fig. 2. Symbols J_A, J_B, and J_C denote the magnitudes of the thrusts while φ_A, φ_B, and φ_C denote the corresponding rotation variables. These thrusts provide control forces in x_b and y_b axes, F_x and F_y respectively acting on the CM, and torque M_z about z_b, according to the linear transformation:

$$\boldsymbol{\tau}_c = \mathbf{B}\mathbf{J} \tag{7a}$$

where

$$\boldsymbol{\tau}_c = [F_x, F_y, M_z]^T \tag{7b}$$

$$\mathbf{B} = \begin{bmatrix} 1 & 0 & 1 & 0 & 1 & 0 \\ 0 & -1 & 0 & -1 & 0 & -1 \\ 0 & -d_{AG} & -d_{DC} & d_{DG} & d_{DC} & d_{DG} \end{bmatrix} \tag{7c}$$

$$\mathbf{J} = [J_A s\varphi_A, J_A c\varphi_A, J_B s\varphi_B, J_B c\varphi_B, J_C s\varphi_C, J_C c\varphi_C]^T \tag{7d}$$

with $s\cdot = sin(\cdot)$, $c\cdot = cos(\cdot)$.

Using the above computations, we derive the equations of motion of the platform in plane motion, expressed in body-fixed frame {B}:

$$\mathbf{M}\dot{\mathbf{v}} = \mathbf{f} + \boldsymbol{\tau}_c \tag{8a}$$

where, the mass and added mass matrix is

$$\mathbf{M} = \begin{bmatrix} m-3m_A & 0 & 0 \\ 0 & m-3m_A & (2d_{DG}-d_{AG})m_A \\ 0 & (2d_{DG}-d_{AG})m_A & I_{zz}-(d_{AG}^2+2d_{BD}^2+2d_{DG}^2)m_A \end{bmatrix} \tag{8b}$$

where m_A is the coefficient of the acceleration in (5), and I_{ZZ} the mass moment of inertia about the z_b axis. Also,

$$\dot{\mathbf{v}} = [\dot{u}, \dot{\upsilon}, \dot{r}]^T \tag{8c}$$

$$\mathbf{f} = [f_x, f_y, f_z]^T \tag{8d}$$

where **f** is a nonlinear function of the velocities of the system not given here due to space limitations.

III. Design Issues

Due to hydrodynamic forces and practical constraints, the shape and the overall size of the platform was given. Nevertheless, the ratio between the base and the side of the isosceles triangular structure, and the location of the platform's center of mass along the symmetry axis, point to two interesting design issues. We study this problem by analyzing **B**, which is a suitable matrix because depends only on platform geometry.

Consider equation (7a), which describes the linear transformation relating the control forces and moment and the jet thrusts. In order to analyze transformation matrix **B**, and make our analysis insensitive to size or unit systems, we normalize (7a) according to

$$\boldsymbol{\tau}_c^* = \mathbf{B}^*\mathbf{J} \tag{9a}$$

where

$$\boldsymbol{\tau}_c^* = [F_x, F_y, (M_z / d_V)]^T \tag{9b}$$

$$\mathbf{B}^* = \begin{bmatrix} 1 & 0 & 1 & 0 & 1 & 0 \\ 0 & -1 & 0 & -1 & 0 & -1 \\ 0 & \frac{-d_{AG}}{d_V} & \frac{-d_{DC}}{d_V} & \frac{d_{DG}}{d_V} & \frac{d_{DC}}{d_V} & \frac{d_{DG}}{d_V} \end{bmatrix} \tag{9c}$$

$$d_V = (L_{AC} + L_{BC})/2 \tag{9d}$$

The normalized matrix $\mathbf{B}^*$ still depends only on platform geometry, and maps the elements of **J** into the force elements of $\boldsymbol{\tau}^*_c$. Next, we investigate its condition number k, i.e. the ratio between the highest and lowest singular value. We choose to work with k, because its value represents a measure of the relation between control values and jet load distribution. Hence, our aim is to keep k as low as possible in order to distribute forces at each jet as equally as possible. The singular values of matrix $\mathbf{B}^*\mathbf{B}^{*\mathrm{T}}$ are found to be:

$$\sigma_2 = \sqrt{3},\ \ \sigma_{1,3} = \frac{\sqrt{3 + d_{AGn}^2 + 2d_{DCn}^2 + 2d_{DGn}^2 \pm \sqrt{K}}}{\sqrt{2}} \tag{10a}$$

where

$$K = (-3 - d_{AGn}^2 - 2d_{DCn}^2 - 2d_{DGn}^2)^2 - 4(2d_{AGn}^2 + 6d_{DCn}^2 + 4d_{AGn}d_{DGn} + 2d_{DGn}^2) \tag{10b}$$

with $d_{XYn} = d_{XY}/d_V$. Since the extensive search of the singular values shows that the inequality $\sigma_1 \geq \sigma_2 > \sigma_3$ is always true, the condition number k of matrix $\mathbf{B}^*\mathbf{B}^{*\mathrm{T}}$ is equal to σ_1/σ_3. Further investigation of k in reasonable limits (L_{AB} = 45m, and 20m < L_{BC} < 70m) results in the following conclusion. The condition number k is minimum when, (a) L_{BC} is minimum, and (b) the ratio $r = d_{AG}/(d_{AG}+d_{DG})$ is equal to 2/3 (see Fig. 2). Note, that for every value of L_{BC} within the search area, k has local minimum when the ratio r is equal to 2/3, see Fig 4.

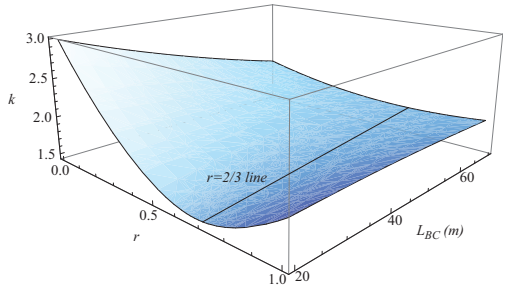

Fig. 4. Condition number k as a function of r and L_{BC}.

Due to space and practical implementation constraints, it was not possible to construct the platform with minimum L_{BC}, but r is very close to optimum.

IV. Closed Loop Control Design

In this section, we design a closed loop controller for

dynamic positioning purposes. We assume as closed control input the vector $\boldsymbol{\tau}_c$. In the next section we transform this in jet **J** vector requirements. From (8a) it is

$$\dot{\mathbf{v}} = \mathbf{M}^{-1}(\mathbf{f} + \boldsymbol{\tau}_c) \tag{11}$$

yielding three scalar equations

$$\dot{u} = f_{u1} + f_{u2} F_x \tag{12a}$$

$$\dot{\upsilon} = f_{\upsilon 1} + f_{\upsilon 2} M_z + f_{\upsilon 3} F_y \tag{12b}$$

$$\dot{r} = f_{r1} + f_{r2} F_y + f_{r3} M_z \tag{12c}$$

where the various f's are functions of the states. We observe that there are input couplings in (12b) and (12c) but the corresponding coefficients $f_{\upsilon 2}$ and f_{r2} are very small, justifying the consideration of $f_{\upsilon 2} M_z$ and $f_{r2} F_y$ as small disturbances that are bounded and that can be counteracted by a robust closed loop controller. Hence, in the last two equations the control design variables are F_y and M_z respectively. Setting

$$F_x = 1/f_{u2}(\alpha - f_{u1} f_{u2}) \tag{13a}$$

$$F_y = 1/f_{\upsilon 3}(\beta - f_{\upsilon 1} f_{\upsilon 3}) \tag{13b}$$

$$M_z = 1/f_{r3}(\gamma - f_{r1} f_{r3}) \tag{13c}$$

with α, β, and γ auxiliary control design variables, we have the system

$$\dot{u} = \alpha \tag{14a}$$

$$\dot{\upsilon} = \beta + f_{\upsilon 2} M_z \tag{14b}$$

$$\dot{r} = \gamma + f_{r2} F_y \tag{14c}$$

From (1a) we can write

$$\ddot{\mathbf{x}} = \dot{\mathbf{R}}\mathbf{v} + \mathbf{R}\dot{\mathbf{v}} \tag{15}$$

Setting the control variables α, β, and γ from (14) as

$$\dot{\mathbf{v}} = \mathbf{R}^T(\mathbf{f}_{fb} - \dot{\mathbf{R}}\mathbf{v}), \tag{16}$$

selecting the feedback such as to include integral action, i.e.

$$\begin{aligned}\mathbf{f}_{fb} = {} & [\ddot{x}_R, \ddot{y}_R, \ddot{\psi}_R]^T - \mathbf{K}_D[\dot{x} - \dot{x}_R, \dot{y}_R - \dot{y}_R, \dot{\psi} - \dot{\psi}_R]^T \\ & - \mathbf{K}_P[x - x_R, y_R - y_R, \psi - \psi_R]^T \\ & - \mathbf{K}_I \int_0^t [x - x_R, y_R - y_R, \psi - \psi_R]^T \, dt\end{aligned} \tag{17}$$

and using the following positive definite diagonal gain matrices $\mathbf{K}_D = diag\{k_{dx}, k_{dy}, k_{d\psi}\}$, $\mathbf{K}_P = diag\{k_{px}, k_{py}, k_{p\psi}\}$, and $\mathbf{K}_I = diag\{k_{ix}, k_{iy}, k_{i\psi}\}$, then the controlled system becomes,

$$\begin{aligned}\ddot{x} - \ddot{x}_R = {} & -k_{dx}(\dot{x} - \dot{x}_R) - k_{px}(x - x_R) \\ & - k_{ix} \int_0^t (x - x_R)\, dt + \varepsilon_x\end{aligned} \tag{18a}$$

$$\begin{aligned}\ddot{y} - \ddot{y}_R = {} & -k_{dy}(\dot{y} - \dot{y}_R) - k_{py}(y - y_R) \\ & - k_{iy} \int_0^t (y - y_R)\, dt + \varepsilon_y\end{aligned} \tag{18b}$$

$$\begin{aligned}\ddot{\psi} - \ddot{\psi}_R = {} & -k_{d\psi}(\dot{\psi} - \dot{\psi}_R) - k_{p\psi}(\psi - \psi_R) \\ & - k_{i\psi} \int_0^t (\psi - \psi_R)\, dt + \varepsilon_\psi\end{aligned} \tag{18c}$$

In (18), "R" denotes a reference (desired) variable, and ε_x, ε_y and ε_ψ are small and bounded disturbances.

V. Control Allocation

In this section, the proposed control allocation scheme that has been implemented is illustrated. The goal is to distribute the closed-loop control forces and moments efficiently to the actuators in such a way that the control objective is realized without violating thruster capabilities.

Equation (7) describes the linear transformation between the vector $\mathbf{J}=[J_A s\varphi_A, J_A c\varphi_A, J_B s\varphi_B, J_B c\varphi_B, J_C s\varphi_C, J_C c\varphi_C]^T$, and the control variables $\boldsymbol{\tau}_C=[F_x, F_y, M_z]^T$. In order to realize the control algorithm described above, we calculate **J**, using (7a), according to:

$$\mathbf{J} = \mathbf{B}^+ \boldsymbol{\tau}_c \tag{19}$$

where $\mathbf{B}^+ = \mathbf{B}^T(\mathbf{B}\mathbf{B}^T)^{-1}$ is the pseudo-inverse of matrix **B**, and the obtained solution locally minimizes the norm of **J**'s elements. Note here that since the system is over-actuated, infinite solutions exist to (7a). Utilizing the presence of redundant actuation controls, (19) can be modified by the addition of the homogenous solution:

$$\mathbf{J} = \mathbf{B}^+ \boldsymbol{\tau}_c + (\mathbf{I} - \mathbf{J}^+\mathbf{J})\mathbf{J}_0 \tag{20}$$

For example, would be a suitable solution in the case, we need $\boldsymbol{\tau}_C = [0, 0, 0]^T$, when the jet thrusts cannot be zero due to diesel engine constraints. However, in this work we assume that this is not the case; therefore we employ the solution described in (19).

Next, from (7) and (19) we calculate the desired magnitudes and angles of the jet thrusts according to the following equations.

$$\begin{aligned}J_{q,des} &= \sqrt{(J_q s\varphi_q)^2 + (J_q c\varphi_q)^2} \\ \varphi_{q,des} &= a\tan 2(J_q s\varphi_q, J_q c\varphi_q)\end{aligned} \tag{21}$$

where $q=A, B, C$. However, the desired values calculated in (21) cannot be supplied immediatly because of actuator dynamics. Here, we model the dynamic of the jets angle according to:

$$\dot{\varphi}_q = (1/t_s)(\varphi_{q,des} - \varphi_q) \tag{21}$$

where t_s is the model's time constant. In addition, according to the specifications, the thrust of each jet is limited to 15kN.

VI. Simulation Results

Our goal in this example is to stabilize the floating platform position in a circle with center in (0,0) and a radius equal to 5m, and the platform direction in 0 deg, with a tolerance equal to ±5 deg. The initial errors are set as x_e = 6.0, y_e = -2.5, in m, ψ_e = -5 deg, u_e = 0.1, v_e = 0.0, in m/s, and, r_e = 0.01 in rad/s. Note, that sensor noise (according to our hardware specifications) is added to position and orientation readings.

A. Without Environmental Disturbances

In this section we present simulation results to demonstrate the performance of the controlled dynamical

system without environmental disturbances. Some characteristic parameters used are given: geometric data L_{AB} = 45, L_{BC} = 35, $m = 42\times510^3$, R_{uc} = 2.2, H_{uc} = 6.5, R_{lc} = 3.5, H_{lc} = 3.0, all in SI units and the hydrodynamic coefficients are C_D = 0.8, C_A = 0.8. The gains of the controller were chosen as $k_{dx} = k_{dy}$ = 0.5, $k_{d\psi}$ = 0.3, $k_{px} = k_{px} = k_{py}$ = 0.2, and $k_{ix} = k_{ix} = k_{iy}$ = 0.0 i.e., no integral action is implemented initially. In Fig. 5, the resulting trajectory of the CM of the platform in the inertial 2D space is displayed.

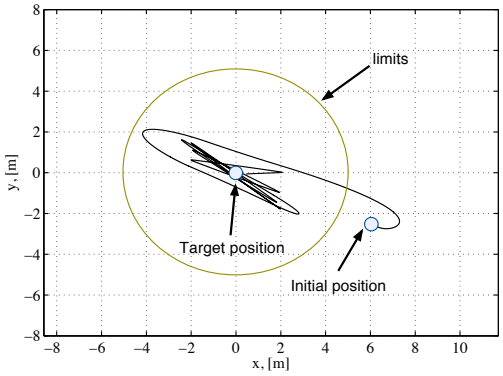

Fig. 5. The 2D path of the CM of the platform.

The linear and angular velocities are depicted in Fig. 6 (a, c, and e,) while in Fig. 6 (b, d, and f) we see the position and orientation variables. Despite the saturation of the jet thrusts, and the finite velocity of the jet rotation, we observe that the platform is stabilized within the required limits.

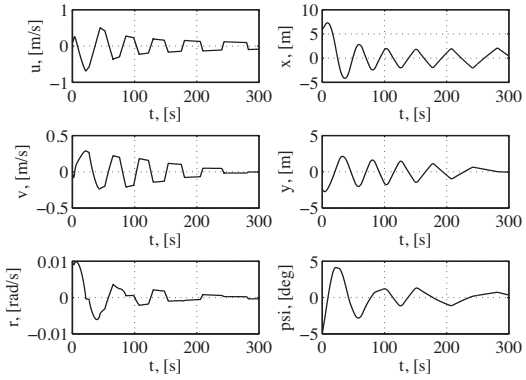

Fig. 6. (a), (c), (e) Linear and angular velocities, and (b), (d), (f) Position and orientation variables.

B. With Environmental Disturbances

Next, simulation results with wind and sea current disturbances are presented. Wind forces (surge and sway) and moment (yaw) are calculated according to:

$$X_{wind} = \frac{1}{2} C_X(\gamma_R)\rho_w V_R^2 A_T \tag{22a}$$

$$Y_{wind} = \frac{1}{2} C_Y(\gamma_R)\rho_w V_R^2 A_L \tag{22b}$$

$$T_{wind} = \frac{1}{2} C_T(\gamma_R)\rho_w V_R^2 A_L L \tag{22c}$$

where C_X and C_Y are the force coefficients and C_T is the moment coefficient. They are functions of the relative angle, γ_R, between the wind and platform direction, and are taken from tables. ρ_w is the density of air in kg/m^3, A_T and A_L are the transverse and lateral projected areas in m^2, and L is the overall length of the platform in m. V_R is the relative wind speed (Fig. 7), and is given in knots, see [13] and [14]. We also impose a sea current with velocity (in m/s) shown in Fig 7. In order to improve the performance of the controller so as to counterbalance environmental disturbances, we activate the integral part of the controller setting $k_{ix} = k_{ix} = k_{iy}$ = 0.01.

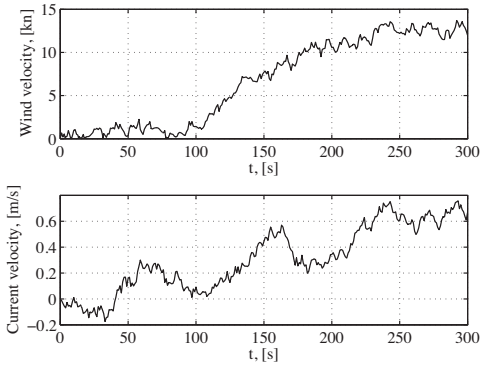

Fig. 7. Wind and sea current velocities.

In Fig. 8, the dynamic positioning performance of the controller is illustrated against the environmental disturbances.

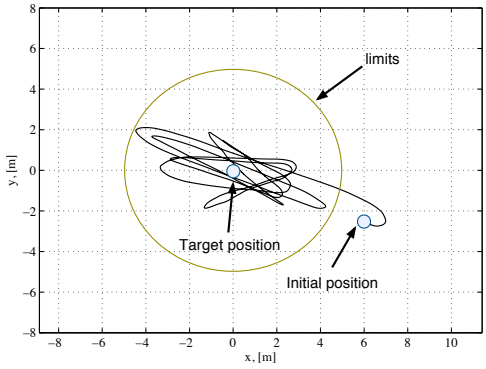

Fig. 8. Dynamic positioning with environmental disturbances.

Fig. 9 (a, b, c, d, e, and f) shows the thrusts of the jets and the corresponding angles. The linear and angular velocities are depicted in Fig. 10 (a, c, and e,) while in Fig. 10 (b, d, and f) we see the position and orientation variables. Again, despite the disturbances and the actuators constraints, the platform is stabilized within the required limits.

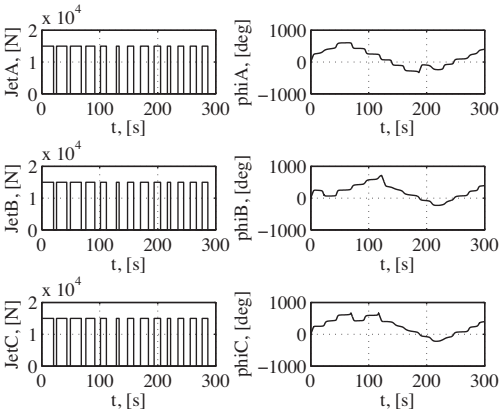

Fig. 9. (a), (c), (e) Jet thrusts, and (b), (d), (f) Jet angles (with environmental disturbances).

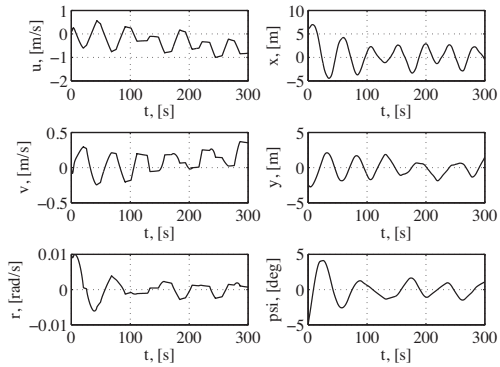

Fig. 10. (a), (c), (e) Linear and angular velocities, and (b), (d), (f) Position and orientation variables (with environmental disturbances).

VII. Practical Implementation

For the implementation of the above described control system, we utilize three GPS receivers, and two antennas, see Fig. 11a and Fig. 11b respectively, which provide the position and orientation of the platform. Two RTK GPS receivers are connected with the antennas and give the orientation data. The position is supplied from the third GPS receiver, which is connected also with one of the antennas. The GPS receivers have an accuracy of ±1 m.

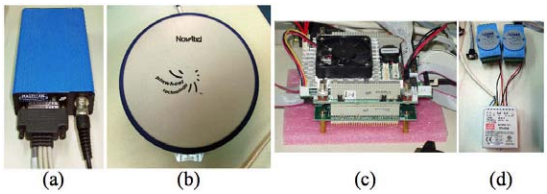

Fig. 11. (a) GPS receiver. (b) Antenna. (c) PC104 control station. (d) Analog output modules with power supply.

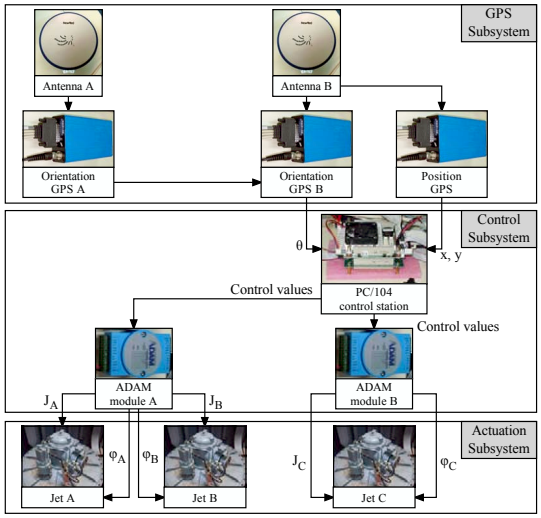

Fig. 12. Structure of the implemented system.

The signals of the GPS receivers are transmitted to the control station via RS232 ports. The control station is a PC104 tower consisting of a cpu module and a module with four RS232 ports, see Fig. 11c. The control station is operated by the real time linux operating system Xenomai. The control algorithm and allocation scheme is coded using the C programming language. The software has as input the position and orientation of the platform and calculates according to the above described algorithms, the desired jet thrusts and angles. The output values control the analog modules (Fig. 11d), which drive the jets. The implemented system, whose structure is depicted in Fig. 12, will be integrated in the platform when its construction is finished. This will allow us to try the controller in the field.

VIII. Conclusion

This paper reports the implementation of an autonomous dynamic positioning scheme of a new triangular floating platform, with real time capabilities. The system is over-actuated, i.e., it has more control inputs than DOF. Hence, we designed an appropriate control allocation scheme in order for the control objective to be realized without violating thruster capabilities. This scheme is based on the pseudo-inversion of the transformation matrix relating the control forces and the jets thrust. In addition, we formulated design rules that maximize the manipulability of the platform, based on the condition number of the normalized transformation matrix relating the control forces and the jets thrust. The methodology provides a fast, reliable, and computationally inexpensive algorithm compared to the complex, on-line, iterative ones. Simulation results, including environmental disturbances, were presented to demonstrate the performance of the controller and allocation scheme.

References

[1] J. F. Wilson, "Dynamics of Offshore Structures," New Jersey, John Wiley and Sons, 2003.

[2] F. E. Hawary (Ed.), "The Ocean Engineering Handbook," Boca Raton, Florida, CRC Press, 2001.

[3] T. I. Fossen, and T. A. Johansen, "A Survey of Control Allocation Methods for Ships and Underwater Vehicles," in *Proc. Mediterranean Control Conference 2006*, 2006.

[4] M. Bodson, "Evaluation of Optimization Methods for Control Allocation," *Journal of Guidance, Control and Dynamics*, vol. 25, pp. 703–711, 2002.

[5] W. C. Webster and J. Sousa, "Optimum Allocation for Multiple Thrusters," *Proc. of the Int. Society of Offshore and Polar Engineers Conference (ISOPE'99)*, Brest, France, 1999.

[6] T. A. Johansen, T. I. Fossen, and S. P. Berge, "Constraint Nonlinear Control Allocation with Singularity Avoidance using Sequential Quadratic Programming," *IEEE Transactions on Control Systems Technology*, vol. TCST-12, pp. 211–216, 2004.

[7] S. P. Berge and T. I. Fossen, "Robust control allocation of over-actuated ships: Experiments with a model ship," *Proc. 4th IFAC Conf. Manoeuvring and Control of Marine Craft*, Brijuni, Croatia, 1997, pp. 166–171.

[8] O. J. Sørdalen, "Optimal Thrust Allocation for Marine Vessels," *Control Engineering Practice*, vol. 5, no. 9, pp. 1223–1231, 1997.

[9] K. M. Lynch, "Controllability of a Planar Body with Unilateral Thrusters," *IEEE Transactions on Automatic Control*, vol. 44, pp. 1206–1211, 1999.

[10] F. Repoulias, K. Vlachos, and E. Papadopoulos, "Modeling and Control of a Triangular Floating Platform Driven by Rotating Jets," in *Proc. 16th Mediterranean Conference on Control and Automation (MED 2008)*, Ajaccio, France, June 25-27, 2008.

[11] nestor.noa.gr

[12] S. F. Hoerner, "Fluid-Dynamic Drag," Hoerner Publications, 1965.

[13] R. M. Isherwood, "Wind Resistance of Merchant Ships," *RINA Trans.*, vol. 115, pp. 327-338, 1972.

[14] T. I. Fossen, "Guidance and Control of Ocean Vehicles," John Wiley & Sons, 1994.